Journal of Solid State Chemistry 230 (2015) 374–380

Contents lists available at ScienceDirect

Journal of Solid State Chemistry

journal homepage: www.elsevier.com/locate/jssc

Intercalation of organic molecules in 2D copper (II) nitroprusside: Intermolecular interactions and magnetic properties

H. Osiry [a], A. Cano [a], A.A. Lemus-Santana [a], A. Rodríguez [a], R.E. Carbonio [b], E. Reguera [a,*]

[a] Centro de Investigación en Ciencia Aplicada y Tecnología Avanzada, Unidad Legaria, Instituto Politécnico Nacional, Mexico
[b] INFIQC-CONICET, Departamento de Físico Química, Facultad de Ciencias Químicas, Universidad Nacional de Córdoba, X5000HUA Córdoba, Argentina

ARTICLE INFO

Article history:
Received 12 May 2015
Received in revised form
24 June 2015
Accepted 27 July 2015
Available online 29 July 2015

Keywords:
2D copper nitroprusside
Intercalation of organic molecules
Intermolecular interactions
Hybrid inorganic–organic solids
Molecular magnets

ABSTRACT

This contribution discusses the intercalation of imidazole and its 2-ethyl derivative, and pyridine in 2D copper nitroprusside. In the interlayer region, neighboring molecules remain interacting throu gh their dipole and quadrupole moments, which supports the solid 3D crystal structure. The crystal structure of this series of intercalation compounds was solved and refined from powder X-ray diffraction patterns complemented with spectroscopic information. The intermolecular interactions were studied from the refined crystal structures and low temperature magnetic measurements. Due to strong attractive forces between neighboring molecules, the resulting π–π cloud overlapping enables the ferromagnetic coupling between metal centers on neighboring layers, which was actually observed for the solids containing imidazole and pyridine as intercalated molecules. For these two solids, the magnetic data were properly described with a model of six neighbors. For the solid containing 2-ethylimidazole and for 2D copper nitroprusside, a model of four neighbors in a plane is sufficient to obtain a reliable data fitting.

1. Introduction

The coordination chemistry provides an elegant route to obtain materials from previously prepared building units. From the assembling of molecular blocks through metal centers, one-dimensional (1D), two-dimensional (2D) and tri-dimensional (3D) materials, with predictable and tunable functional properties can be designed and prepared. The properties of the resulting solids are determined by those of the involved building units, the molecular blocks and the metal centers that are coordinating them. Metal-organic frameworks (MOFs), a family of porous 3D materials prepared from organic blocks coordinated by metal centers, are illustrative examples on the scope and diversity of materials prepared from coordination chemistry routes. The potentiality of MOFs in gases storage adsorption and separation [1], heterogeneous catalysis [2], controlled drug delivery [3], sensors [4], environmental remediation [5], energy storage [6], and biomedical applications [7] are well known. From square planar building blocks, and even, from tetrahedral and octahedral ones, the preparation of 2D solids is possible. Layered (2D) materials are characterized by high values for the specific surface, for some cases, with all the involved atoms located at their surface. The high catalytic activity of 2D solids, for instance, is closely related to such structural features [8]. The exfoliation of 2D materials, using appropriate solvents or physical methods, leads to single layer crystals with unique structural, electrical, optical, magnetic, thermal and mechanical properties [9–12]. From the re-assembling of these single layer crystals followed by their combination with 1D solids, 3D materials and devices with unexpected functional properties can be prepared [13–15].

From the intercalation of molecular blocks (1D) in layered (2D) coordination polymers, hybrid inorganic–organic 3D frameworks result. Such materials can be seen as atomic level buildings formed from layers separated by regularly located organic pillars to form 3D crystals. With appropriate election of building blocks, porous solids with tunable pore size, geometry and functionality are obtained [16,17]. Their functionality is determined by the functional group found at the pore surface, the framework flexibility, and the cooperative interactions of neighboring layers through the intercalated molecules [18]. Such solids have potential applications for instance, in pressure-controlled gas adsorption and separation [19], controlled drug release [20], and as tunable molecular magnets [21]. The intercalation of organic molecules in layered solids provides a useful model to study the non-covalent intermolecular interactions because the intercalated molecules remain confined to a small volume region, under restricted molecular configurations, and interacting with only a limited number of neighboring molecules.

In this contribution, we discuss the intercalation of heterocycle organic molecules containing a pyridinic N atom (imidazole and 2-ethyl derivative, and pyridine), between layers of copper

* Corresponding author.
E-mail address: edilso.reguera@gmail.com (E. Reguera).

http://dx.doi.org/10.1016/j.jssc.2015.07.042
0022-4596/

nitroprusside (2D) [22] to form 3D framework supported on intermolecular interactions. The presence of the pyridinic N atom in the molecule ring enables its coordination to the metal centers at the layer. The crystal structure of the resulting hybrid inorganic–organic solids was solved and refined from powder X-ray diffraction (PXRD) complemented with information from XRF, IR, UV–vis and thermogravimetric (TG) measurements. In the resulted 3D hybrid solids, neighboring layers remain communicated through intermolecular interactions between intercalated molecules. In the interlayer region the molecules remain interacting through their dipole and quadrupole moments, and for relatively strong attractive forces (short ring–ring distance), the π–π clouds overlapping makes possible the ferromagnetic coupling between metal centers from neighboring layers [23,24]. Such interaction was studied from low temperature magnetic measurements. To the best of our knowledge, this is the first study on the intercalation of organic molecules in the metal nitroprussides series.

2. Experimental

All the reagents used were analytical grade products from Sigma-Aldrich. The layered phase of copper (II) nitroprusside, $Cu(H_2O)_2[Fe(CN)_5NO]$, was prepared by the precipitation method, from diluted aqueous solutions of copper nitrate and of sodium nitroprusside [22]. The precipitate was washed several times with distilled water, and finally dried at room conditions until it had constant weight. The nature and purity of the obtained green powder were tested from IR and PXRD data. The layered solid (2D) was suspended in an ethanol/water mixture (1:1 v/v) and the molecules to be intercalated (L) added dropwise under constant stirring. The molar ratio used of the 2D solid to the molecules to be intercalated (L), was 1:2, which corresponds to the expected formula unit, $CuL_2[Fe(CN)_5NO]$. For imidazole and its derivatives, the molecular solid was dissolved in ethanol (0.01 M). The solid resulting from the intercalation process was aged for a week within the mother liqueur, then separated by centrifugation, washed several times with distilled water, and finally air-dried until it had constant weight. It was then characterized from PXRD, XRF, IR, UV–vis and TG measurements.

IR and UV–vis spectra were recorded by the ATR and integration sphere method, respectively, using Perkin-Elmer equipment. TG curves were collected under an N_2 flow (1 L/min) using a TA Instruments (IR-5000) equipment operated in the HR mode. PXRD patterns were recorded in the Bragg-Brentano geometry using $CuK_{\alpha 1}$ radiation and a D8 Advance diffractometer (from Bruker) equipped with a Lynx eye detector and germanium monochromator. The unit cell was identified with the help of DICVOL program [25]. For the structural study, the diffraction pattern was decomposed, in term of extracted intensities, by the Le Bail procedure using pseudo-Voigt peak profile function [26]. Peak profiles were calculated within ten times the full width at half maximum (FWHM). The background was modeled by at third-order polynomial. The structural model to be refined was derived by a combination of direct and heavy atom methods implemented in the SHELX program [27]. The structural model was completed from the analysis of the corresponding electron density Fourier maps. The crystal structure was finally refined with the Rietveld method implemented in the FullProf program [28]. The interatomic C–N and Ni–C distances within the layer were constrained to take values within certain limits considering the reported crystal structure for 2D copper(II) nitroprusside [22]. Details on the PXRD data recording and processing are available from Supplementary material.

The low temperature zero field cooling/ field cooling (ZFC/FC) curves were collected under an applied field of 50 Oe, with a MPMS-3 magnetometer from Quantum Design. The magnetization curves versus applied magnetic field were recorded in the −6 to 6 T range at 2 K. From the ZFC/FC curves, the χT versus T dependences were calculated and then fitted using PHI program [29] in order to confirm the interaction model suggested by the structural study. The dipole and quadrupole moments for imidazole, 2-ethyl derivatives and pyridine, as isolated molecules, were calculated using Gaussian 09 software with DFT method using B3LYP functional and 6–21 g+(d,p) base.

3. Results and discussion

3.1. Crystal structure

Table 1 summarizes the unit cell parameters, cell volume and space group found for the hybrid solids resulting from the intercalation of imidazole (Im), 2-ethylimidazole (EtIm), and pyridine (Py) in 2D copper (II) nitroprusside. Fig. 1 shows the experimental PXRD pattern and its fitting, according to the refined structural model, for the solid containing imidazole as intercalated species. Analogue pattern fittings were obtained for the solid containing the remaining molecules (Supplementary information). The refined atomic positions and thermal and occupation factors, and the calculated bond distances and angles, are available from Supplementary information and were deposited in the CCDC database with the file numbers indicated below. Fig. 1 (Inset) illustrates the coordination environment for the involved metal centers and the used atoms labels. Table 2 summarizes the molecule dipole and quadrupole moments and the relevant interatomic distances and angles, particularly, the $Cu–N_{mol}$ and ring–ring distances and the ring–ring angle. Figs. 2, 3 and 4 show the atomic packing within the unit cell for the solids containing Im, EtIm and Py as intercalated molecules. The intercalated molecules were found coordinated to the axial positions for the copper atom. In the interlayer region, neighboring molecules remain interacting through their dipole and quadrupole moments, but with different intermolecular configuration.

For imidazole, the orientation of the molecular dipole moment and the molecule dipolar coupling, is forcing to a relative shift of neighboring layers in x,y plane of about 3.627 Å. Such shift favors the accommodation of the unlinked CN and NO groups minimizing the repulsive interaction of their electron clouds. For this molecule, related to the intermolecular interaction, the inorganic block adopts a slightly undulated conformation. The ring–ring distance between neighboring molecules was found to be in the 3.57–3.84 Å range, which supposes that a π–π interaction is possible. The calculated ring–ring angle is 161°, a deviation relatively large relative to the coplanar configuration expected in absence of

Table 1
Cell parameters, cell volume per formula unit, unit cell and space group for the hybrid solid under study.

Molecule	Cell parameters, Å	Cell volume per formula unit, Å^3	Space group
Imidazole	a=15.5053(3) b=7.2535(3) c=14.4102(3)	1620.68(8)	$P\,2_1\,2_1\,2_1$
2-ethylimidazole	a=17.6604(4) b=18.6264(2) c=11.0262(3) β=95.590(2)°	2059.41(7)	$P\,2_1/n$
Pyridine	a=13.5597(3) b=18.3476(4) c=7.5551(1) β=93.836(1)°	1875.41(6)	$I\,a$

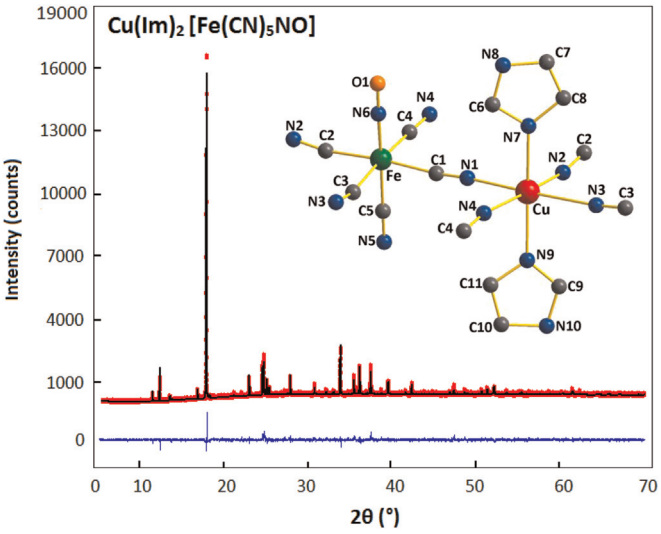

Fig. 1. XRD powder pattern for $Cu(Im)_2[Fe(CN)_5NO]$, its fitting according to the refined structural model, and their difference. Analogs pattern fitting were obtained for EtIm and Py (see Supplementary information). Inset: Coordination environment for the involved metal centers.

repulsive interaction. Such repulsive feature results from the quadrupolar interaction and it was ascribed to the relatively large negative values for the molecule quadrupole moments (Table 2).

For 2-ethylimidazole (Fig. 3), the ring–ring distance is above 5 Å, which suggests that all the intermolecular interaction must be of dipolar nature. This is congruent with the calculated ring–ring angle for the closest molecules, which is 180°. Compared with imidazole, the ethyl derivate has a more negative quadrupole moment and, in the presence of quadrupolar interaction, a large deviation from the coplanar configuration for the rings of neighboring molecules is expected, which was not observed. The orientation of the ethyl residue for the intercalated molecules (Fig. 3) is determined by both, dipolar interaction and steric the factor. This orientation disfavors the octahedral coordination for the cooper atom where only three equatorial CN groups are found coordinated. The cooper atom adopts a distorted square pyramidal geometry defined by two CN groups and the two EtIm molecules. Neighboring layers were found interacting through hydrogen bonds formed between donor N atom of EtIm molecule and the acceptor N and O atoms from the unlinked CN and NO groups at bond distances of 2.700 and 3.062 Å, respectively. Related to the relatively weak intermolecular interaction for EtIm, the inorganic layer adopts a practically flat conformation, similar to the observed for 2D copper (II) nitroprusside. Such structural features for EtIm containing solid, are unique within the considered series of intercalation compounds.

For pyridine, two types of molecules configurations were observed, a sandwich type conformation with ring–ring distance and ring–ring angle of 3.775 Å and 176.5°, respectively, and a parallel-displaced one but with larger ring–ring distance (5.03 Å) (Fig. 4). The existence of these two molecular configurations within the interlayer region for pyridine was attributed to both, steric factors and repulsive interactions with the electron clouds of the axial NO and CN groups. For this molecule, the dipole moment is oriented on the N_{Py}-metal coordination bond, quite different to the one observed for imidazole, which also is a small molecule without substituent group, where the dipole moment forms an angle of 11.72° with the N_{Im}–metal coordination bond. The two configurations found for the pyridine molecules within the interlayer region determine the undulated conformation for the copper (II) nitroprusside layer in the intercalation compound (Fig. 4). The displacement of neighboring layers in the *x,y* plane is *c. a.* 3.777 Å. The presence of parallel-displaced configuration for pyridine in the interlayer region, explains that for this molecule the cell volume per formula unit is higher than the one obtained for imidazole (Table 2).

The $Cu–N_{mol}$ interatomic distance for the coordination bond is determined by both, the electron donating capability of the intercalated molecule and the ability of the metal to receive that electron density, sensed through its effective polarizing power (Ze/r^2). A molecule with a high electron donating capability combined with a high polarizing power for the metal, favor the formation of a stronger coordination bond. According to the values calculated for the $Cu–N_{mol}$ distance, the stronger coordination bond is formed for imidazole and its ethyl derivative. In turn, the ligand charge donation to the metal modifies the polarizing power of this last one, reducing its ability to subtract electron density from the –N≡C-Fe– chain, and modifying the π-back donation from the iron atom.

3.2. Spectroscopic characterization and thermal behavior

The structural study discussed above, was complemented with spectroscopic and thermal data. The intercalation of the organic molecule between layers of the inorganic block was confirmed by the changes in their IR spectra. The assignment of the observed IR absorption bands for 2D copper (II) nitroprusside have already been reported [22]. It is similar to that reported for Hg(I) nitroprusside, which also has a layered structure [30]. Since the intercalated species is replacing the water molecules in the copper atom coordination sphere, the ν(OH) stretching and δ(HOH) bending vibrations from coordinated water molecules disappear (Supplementary information). In the inorganic block, $Cu(H_2O)_2[Fe(CN)_5NO]$, these bands are observed in the 3700–3400 cm^{-1} and 1620–1590 cm^{-1} spectral region, respectively. At the same time, on the coordination bond formation, the molecule donates charge to the metal, which induces changes in its vibrational pattern, appreciated as frequency shifts for the IR absorption bands and in their relative intensities. The charge donation to the metal reduces its polarizing power and, in consequence, decrease the metal ability

Table 2
$Cu–N_{mol}$ and ring–ring distances, ring–ring angle, Curie-Weiss constant (θ_{CW}) and superexchange integral (J) for the series of intercalation compounds under study; and dipole and quadrupole (Q) moments for the involved molecules (L).

L	Dipole, in D	Quadrupole, in D Å	Cu–N_{mol}, in Å	Ring–ring distance, in Å	Ring–ring angle, in deg	θ_{CW}, in K	J, in cm^{-1}
Im	3.8699	Q_{xx}: −23.1404 $Q_{yy:}$ −30.0956 $Q_{zz:}$ −32.4708	Cu-N_7:2.231(4) Cu-N_9:2.233(4)	3.575(5)–3.836(5)	161.15	0.222	−0.13
EtIm	3.7521	Q_{xx}: −38.6847 $Q_{yy:}$ −42.4948 $Q_{zz:}$ −45.1390	Cu-N_7:2.235(6) Cu-N_9:2.243(6)	5.241(3)–5.623(4)	180 59	−0.402	−0.99
Py	2.6893	Q_{xx}: −28.1515 $Q_{yy:}$ −36.6014 $Q_{zz:}$ −38.117	Cu-N_7:2.377(6) Cu-N_8:2.455(6)	3.775(5):sandwich > 5 (parallel-displaced)	176.5	0.266	−0.11

Im: Imidazole; EtIm: 2-ethylimidazole; Py: Pyridine. For $Cu(H_2O)_2[Fe(CN)_5NO]$ the values for J and θ_{CW} are −1.0 cm^{-1} and −2.389 K, respectively.

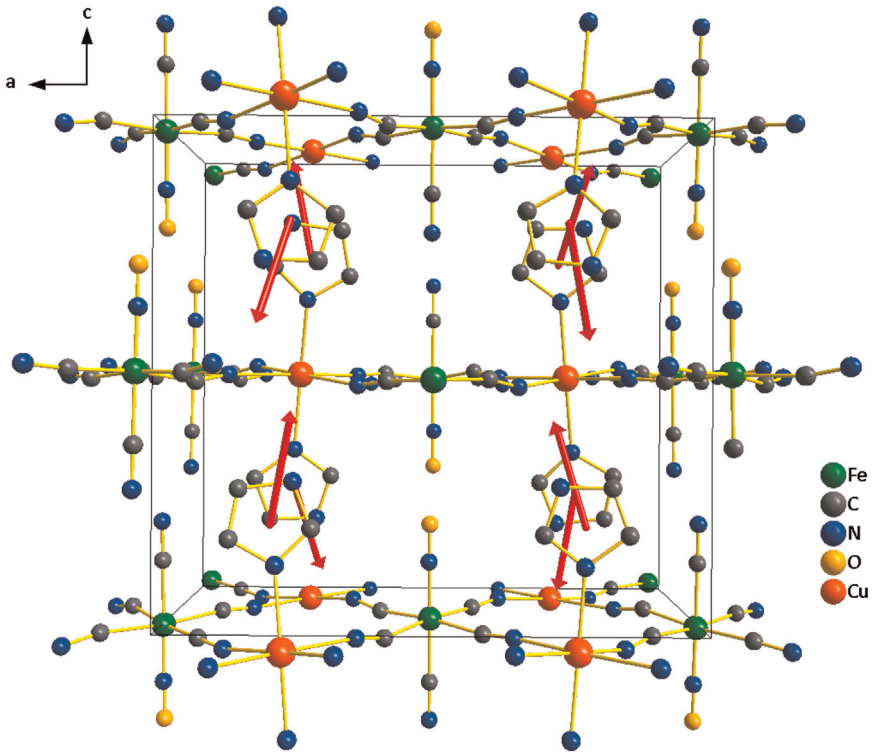

Fig. 2. Atomic packing within the unit cell for the intercalation compound of imidazole in 2D copper (II) nitroprusside. The arrows indicate the dipolar coupling between neighboring molecules.

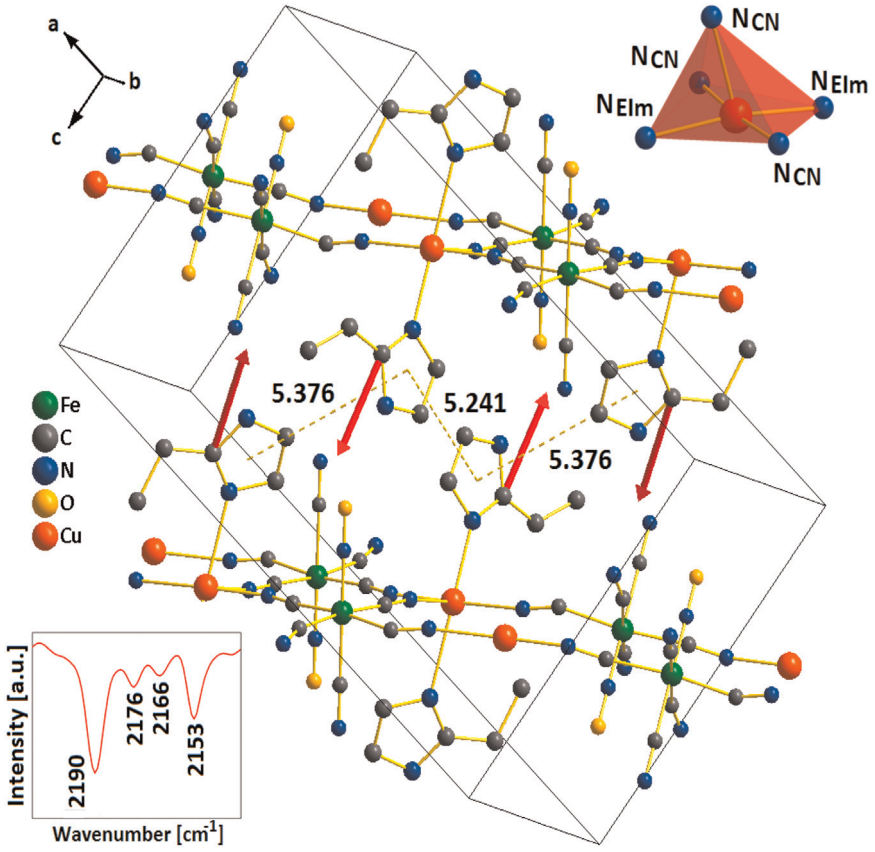

Fig. 3. Atomic packing within the unit cell for the intercalation compound of 2-ethylimidazole in 2D copper (II) nitroprusside. The arrows indicate the dipolar coupling between neighboring molecules. Insets: Coordination polyhedron for the copper atom and ν(CN) stretching region for the IR spectrum.

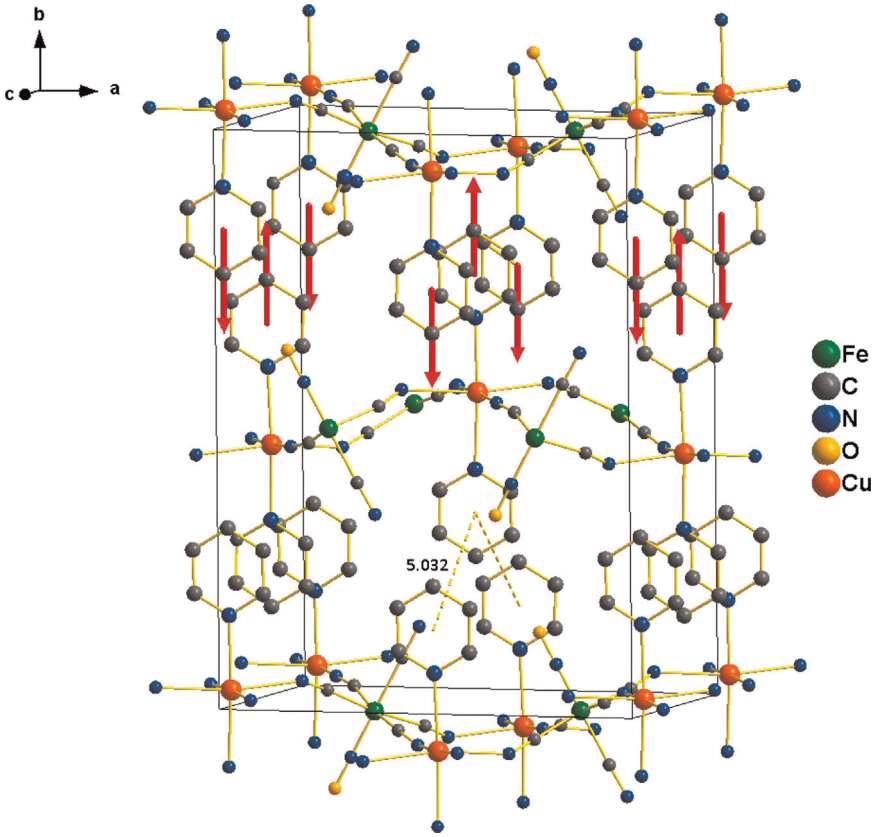

Fig. 4. Atomic packing within the unit cell for the intercalation compound of pyridine in 2D copper (II) nitroprusside. The arrows indicate the dipolar coupling between neighboring molecules.

Table 3
Frequency, in cm^{-1}, for the relevant IR vibrations for copper (II) nitroprusside (2D) and for the hybrid solids obtained by intercalation of the organic molecules (L).

Solid	$\nu(CN)_{eq}$	$\nu(CN)_{ax}$	$\nu(NO)$	Cu–N_{mol}
2D	2220	2161	1950	–
$2D(Im)_2$	2191	2154	1913	305
$2D(EtIm)_2$	2190, 2176, 2166	2153	1929	289
$2D(Py)_2$	2193	2159	1906	275

Im: Imidazole; EtIm: 2-ethylimidazole; Py: Pyridine.

to subtract charge from the CN ligand. This is detected as a negative frequency shift for the ν(CN) stretching vibration of both, the equatorial and axial CN groups (Table 3). Certain frequency shift is also detected for the axial NO group, because the exchange of ligands around the copper atom modifies the charge distribution within the nitroprusside building block (Table 3). Such IR spectral features provide conclusive clue on the organic molecule coordination to the axial positions of the copper atom, in accordance with the structural study. For imidazole and its ethyl derivative, the absence of the broad absorption band, in the 3000–2500 cm^{-1} spectral region (Supplementary information), from the strong hydrogen bridges between the pyrrolic N_1 and the pyridinic N_3 nitrogens of neighboring molecules, which features the molecular crystal, provides an additional evidence for the molecule coordination to the copper atom. That broad band results from Fermi resonance interactions of ν(NH) with forbidden bands (harmonics and combination bands) [31]. That band disappears when the pyridinic nitrogen is coordinated to the metal; in absence of hydrogen bridges, only ν(NH) stretching vibration of the molecule is observed. For EtIm as intercalated molecule, four ν(CN) absorption bands at 2190, 2176, 2166 and 2153 cm^{-1} were observed (Table 1 and Supplementary information). This suggests the existence of also equatorial CN groups as unbridged ligand (discussed below). The ν(CN) band at 2166 cm^{-1} corresponds to the unbridged equatorial CN group, while the band of intermediate frequency, at 2176 cm^{-1}, was ascribed to the CN group in apical position in the copper atom coordination polyhedron (Fig. 3, Inset).

The recorded UV–vis spectra (Supplementary information) are in correspondence with the above-discussed evidence from IR spectroscopy concerning the organic molecule coordination to the copper(II) ion. The absorption bands observed in the visible region, at 605 and 655 nm, correspond to $^2B_{1g} \rightarrow {}^2E_g$ and d–d transitions, respectively, for octahedral copper (II) species. The position (frequency) of these bands is similar to the one observed for the 2D inorganic block (copper (II) nitroprusside dihydrate). The bands below 500 nm, at 209, 257, and 319 nm, were ascribed to 11e→13e, 12e→13e, and 2b2→13e metal–ligand electronic transitions, respectively [32]. The ligand exchange at the axial positions for the copper atom has a detectable effect in these last metal–ligand transitions (Supplementary information). The charge redistribution within the ···Cu–N≡C–Fe··· chain modifies the energy levels separation involved in these transitions.

The recorded TG curves confirmed the formula unit found from the structural study, $CuL_2[Fe(CN)_5NO]$. Four thermal effects related to the ligands evolution on heating were observed, with the appropriate quantitative correspondence of the weight loss according to the expected formula unit (Supplementary information). The thermal decomposition process is promoted by vibration of molecules and ligands induced by the thermal energy (kT), which leads to rupture of the involved chemical bonds and evolution of thermal decomposition products. By this reason, the first species to evolve are those weakly bonded or where the molecular

fragment is highly sensible to the vibrational motion. For the materials under study, that last condition is found for the axial ligands of both, the iron (II) and copper (II) ions. The axial NO and CN groups remain unbridged which favors a relatively high vibrational amplitude around the Fe–N and Fe–C chemical bonds, and this favors their rupture. The thermal decomposition of metal nitroprussides begins with the evolution of the unbridged NO and CN groups [33]. For the axial ligands of the copper (II) ion (the intercalated organic molecules), the interaction between them in the interlayer region, has physical nature, and it could be relatively weak, depending of the molecule dipole and quadrupole moments. For the intercalation compounds herein studied, the first two thermal effects correspond to the evolution of the organic intercalated molecules and to the axial NO and CN groups, in that order, which for imidazole and its ethyl derivative appear unresolved in the 150–200 °C temperature range (Supplementary information). This is confirmed by the IR spectrum for the solid residue of samples heated up to 250 °C, which has no absorption bands for the axial ligands of both, the copper and iron atoms (Supplementary information). For pyridine, these two effects appear partially resolved. Then, at higher temperatures, from 280 °C the equatorial CN groups also evolve in two steps. In the solid residue for samples heated up to 500 °C, the IR spectra show presence of CN groups coordinated to metal centers, presumably to iron (II) ions, according to the frequency for the ν(CN) vibration, which is observed as a strong band at 2027 cm^{-1}. For higher heating temperature, the formation of metallic species is expected, and already observed for the sample heating at 500 °C (Supplementary information). The presence of metallic species in the final products could be explained by the reducing role of the evolved CN radicals, giving C_2N_2. This is a well-known effect in the thermal decomposition of transition metal cyanides [34].

3.3. Magnetic properties

For the considered series of intercalated compounds, there are two possible magnetic interaction between copper atoms. Within the layer it is of antiferromagnetic nature because the iron atom of the nitroprusside building block remains in diamagnetic state (low spin iron(II)). For relatively strong intermolecular interaction within the interlayer region, through the molecule dipole and quadrupole moments, certain overlapping of the π-cloud of neighboring molecules is possible. Such π–π interaction supports the possibility of a ferromagnetic coupling between copper atoms from neighboring layers. Because the intercalation compounds form an ordered 3D framework, such coupling could be observed as a cooperative ferromagnetic ordering at low temperature. This has been observed for Ni and Co through molecules of imidazole and its derivatives intercalated in layered 2D coordination polymers [23,24].

For the series of intercalated solids under study, including the inorganic block, 2D copper (II) nitroprusside, the magnetic susceptibility (χ) was calculated from the recorded zfc/fc curves in order to identify the nature of the observed magnetic behavior. The values obtained for the Curie-Weiss constant (θ_{CW}) are summarized in Table 2. The presence of a possible ferromagnetic interaction was explored recording the magnetization curves under applied field at 2 K (Supplementary information). Fig. 5 shows the zfc/fc curves for imidazole as intercalated molecules. The χ^{-1} versus temperature plot shows a slightly positive intercept (Fig. 5, Inset), which corresponds to presence of a weak ferromagnetic interaction. An analogue behavior was observed for pyridine (see Supplementary information). For 2D copper (II) nitroprusside, the Curie-Weiss constant is negative, −2.39 K, an expected result because for this solid only the antiferromagnetic interaction between the copper atoms in the layer is possible. For the intercalation compound

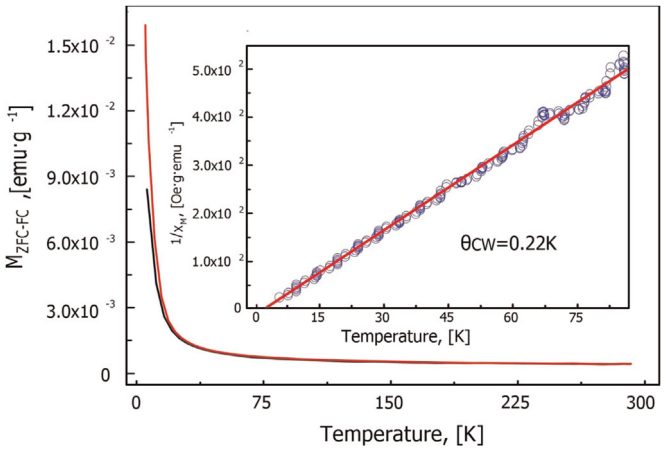

Fig. 5. Zero field cooling/field cooling curves with an applied field of 50 Oe for the intercalation compound of imidazole in 2D copper (II) nitroprusside. Inset: Inverse of susceptibility versus temperature curve.

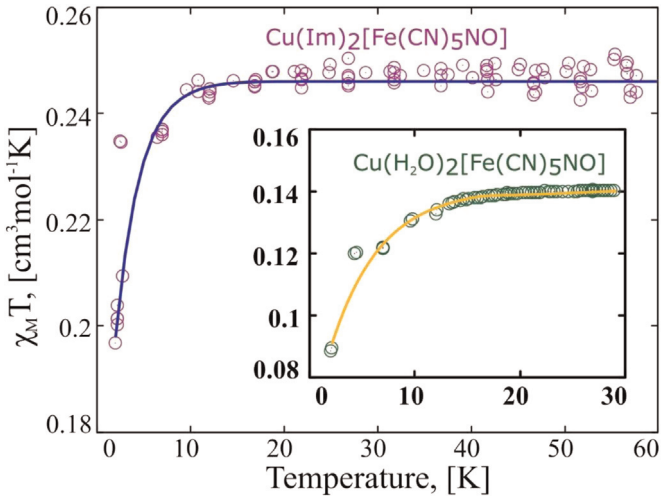

Fig. 6. χT versus T dependence for $Cu(Im)_2[Fe(CN)_5NO]$ and its fitting with a model of six paramagnetic neighbors. Inset: χT versus T dependence for $Cu(H_2O)_2[Fe(CN)_5NO]$ and its fitting with a model of four paramagnetic neighbors.

containing 2-ethylimidazole, also a negative value for θ_{CW} was found (−0.402 K), which corresponds to absence of ferromagnetic interaction. This is consistent with the above-discussed structural features for this solid. The ring–ring distance for the intercalated 2-ethylimidazole molecules is above 5 Å, without possibility of π–π overlapping between them, and from this fact, the observed absence of ferromagnetic interaction through the intercalated molecules. The recorded magnetization curves versus applied field corroborate the information derived from the χ^{-1} versus temperature plots. For imidazole and pyridine, the magnetization curves show a slight but perceptible hysteresis (see Supplementary information).

According to the above-discussed structural study, for imidazole and pyridine, a given copper (II) ion is found interacting with six paramagnetic centers. From this fact, the corresponding χT versus T curves could be fitted using an interaction model of six neighbors. For 2-ethylimidazole, where the magnetic axial interaction through the intermolecular interaction is quite weak, an interaction model based in four metal neighbors in the x,y plane could be used. A similar interaction model is expected for 2D copper nitroprusside dihydrate. Fig. 6 shows the χT versus T curve fitting for $Cu(Im)_2[Fe(CN)_5NO]$ and $Cu(H_2O)_2[Fe(CN)_5NO]$ using an interaction model of six and four neighbors, respectively. Analogue fittings were obtained for the solids containing pyridine and

2-ethylimidazole as intercalated species (see Supplementary information). The values for the superexchange integral (J), derived from these fittings are available from Table 2. The values of J are negative and remain below $-1\,cm^{-1}$, which indicates that the weak antiferromagnetic interaction dominates. The distance between neighboring copper (II) ions within the layer is above 10 Å. The existence of that antiferromagnetic interaction between metal ions separated such large distance is possible by the π-back bonding ability of the CN ligand.

4. Conclusions

Imidazole and its 2-ethyl derivative, and pyridine were intercalated between layers of 2D copper (II) nitroprusside. The intercalated molecules were found coordinated to the axial positions of the copper atom. The crystal structure of the formed 3D solids was solved and refined from XRD powder patterns. In the interlayer region, neighboring molecules remain interacting through their dipole and quadrupole moments. For the herein studied intercalation compounds, two types of magnetic interaction between the copper atoms are possible, antiferromagnetic within the layer and of ferromagnetic nature through the intercalated molecules. For imidazole and pyridine, a weak ferromagnetic interaction was identified, through a positive value for the Curie–Weiss constant. Such behavior results from the π-cloud overlapping of neighboring molecules ring. For 2-ethylimidazole, no ferromagnetic interaction was observed; the Curie–Weiss constant is negative, similar to the value found of that parameter for layered copper (II) nitroprusside. For this imidazole derivative, the ring–ring distance is above 5 Å, without possibility to have overlapping between their π-clouds.

Supplementary information

CCDC files containing the supplementary crystallographic data for $Cu(Im)_2[Cu(CN)_5NO]$: 1034151; $Cu(EtIm)_2[Cu(CN)_5NO]$: 1034152; $Cu(Py)_2[Cu(CN)_5NO]$: 1034153. These data can be obtained from http://www.ccdc.cam.ac.uk/conts/retrieving.html, and also from the Cambridge Crystallographic Data Centre, 12 Union-Road, Cambridge CB21EZ, UK; fax: (+44)1223-336-033; or e-mail: deposit@ccdc.cam.ac.uk.

Acknowledgments

This study was partially supported by the CONACyT (Mexico) projects 2011-01-174247, 2011-01-166387, CONACyT-SENER 231461, and SRE-2013-191089. R.E.C. thanks FONCYT for a cooperation program with CONACYT: PICT2012-3079, CONICET and SECYT-UNC. The authors thank Dr. C. I. Aguirre for the dipole and quadrupole moments calculation for pyridine, imidazole and 2-ethyl imidazole.

Appendix A. Supplementary material

Supplementary data associated with this article can be found in the online version at http://dx.doi.org/10.1016/j.jssc.2015.07.042.

References

[1] X. Lin, J. Jia, X. Zhao, K.M. Thomas, A.J. Blake, G.S. Walker, N.R. Champness, P. Hubberstey, M. Schröder, Angew. Chem. Int. Ed. 45 (2006) 7358.
[2] A. Corma, H. García, F.X. Llabrés i Xamena, Chem. Rev. 110 (2010) 4606.
[3] P. Horcajada, C. Serre, G. Maurin, N.A. Ramsahye, F. Balas, M. Vallet-Regí, M. Sebban, F. Taulelle, G. Férey, J. Am. Chem. Soc. 130 (2008) 6774.
[4] L.E. Kreno, K. Leong, O.K. Farha, M. Allendorf, R. Van Duyne, J.T. Hupp, Chem. Rev. 112 (2011) 1105.
[5] E. Barea, C. Montoro, J.A.R. Navarro, Chem. Soc. Rev. 43 (2014) 5419.
[6] Sh-L. Li, Q. Xu, Energy Environ. Sci. 6 (2013) 1656.
[7] N.J. Hinks, A.C. McKinlay, B. Xiao, P.S. Wheatley, R.E. Morris, Micropor. Mesopor. Mater. 129 (2010) 330.
[8] U. Díaz, A. Corma, Dalton Trans. 43 (2014) 10292.
[9] J.N. Coleman, M. Lotya, A. O'Neill, S.D. Bergin, P.J. King, U. Khan, K. Young, A. Gaucher, S. De, R.J. Smith, et al., Science 331 (2011) 568.
[10] Y. Hernandez, V. Nicolosi, M. Lotya, F.M. Blighe, Z. Sun, S. De, I.T. McGovern, B. Holland, M. Byrne, Y.K. Gunko, et al., Nat. Nanotechnol. 3 (2008) 563.
[11] K.-A.N. Duerloo, M.T. Ong, E.J. Reed, J. Phys. Chem. Lett. 3 (2012) 2871.
[12] V.K. Rao, M.A. Green, S.K. Pati, S. Natarajan, J. Phys. Chem. B 111 (2007) 12700.
[13] H.O. Pastore, L. Marchese, J. Mater. Chem. 19 (2009) 2453.
[14] J.K. Bera, K.R. Dunbar, Angew. Chem. Int. Ed. 41 (2002) 453.
[15] V.P. Georgiev, J.E. McGrady, Inorg. Chem. 49 (2010) 5591.
[16] J.T. Culp, C. Madden, K. Kauffman, F. Shi, C. Matranga, Inorg. Chem. 52 (2013) 4205.
[17] J.T. Culp, S. Natesakhawat, M.R. Smith, E. Bittner, C. Matranga, B. Bockrath, J. Phys. Chem. C 112 (2008) 7079.
[18] Y. Hijikata, S. Horike, M. Sugimoto, M. Inukai, T. Fukushima, S. Kitagawa, Inorg. Chem. 52 (2013) 3634.
[19] Z.-H. Xuan, D.-S. Zhang, Z. Chang, T.-L. Hu, X.-H. Bu, Inorg. Chem. 53 (2014) 8985.
[20] X. Bi, H. Zhang, L. Dou, Pharmaceutics 6 (2014) 298.
[21] X.-Y. Wang, Z.-M. Wang, S. Gao, Chem. Commun. (2007) 1127.
[22] A. Gómez, J. Rodríguez-Hernández, E. Reguera, J. Chem. Cryst. 34 (2004) 893.
[23] M. González, A.A. Lemus-Santana, J. Rodríguez-Hernández, M. Knobel, E. Reguera, J. Solid State Chem. 197 (2013) 317.
[24] M. González, A.A. Lemus-Santana, J. Rodríguez-Hernández, C.I. Aguirre-Vélez, M. Knobel, E. Reguera, J. Solid State Chem. 204 (2013) 128.
[25] D. Louer, R. Vargas, J. Appl. Crystallogr. 15 (1982) 540.
[26] A.L. Le Bail, ESPOIR: A Program for Solving Structures by Monte Carlo from Powder Diffraction Data, in EPDIC-7, Barcelona, 2000. ⟨http://www.cristal.org/sdpd/espoir/SS⟩.
[27] G.M. Sheldrick, Program for Crystal Structure Determination, Institute fur Anorg, Chemie, Göttingen, Germany, 1997.
[28] J. Rodríguez-Carvajal, FullProf 2005 Program, Institute Louis Brillouin, Saclay, France, 2005.
[29] N.F. Chilton, R.P. Anderson, L.D. Turner, A. Soncini, K.S. Murray, J. Comput. Chem. 34 (2013) 1164.
[30] H. Osiry, A. Cano, L. Reguera, A.A. Lemus-Santana, E. Reguera, J. Solid State Chem. 221 (2015) 79.
[31] S. Scheiner, M. Yi, J. Phys. Chem. 100 (1996) 9235.
[32] P.T. Manoharan, H.B. Gray, J. Am. Chem. Soc. 87 (1965) 3340.
[33] J. Rodríguez-Hernández, L. Reguera, A.A. Lemus-Santana, E. Reguera, Inorg. Chim. Acta 428 (2015) 51.
[34] R. Robinette, R.L. Collins, J. Coord. Chem. 4 (1974) 65.